



UNIVERSITAT POLITÈCNICA DE CATALUNYA
BARCELONATECH

Escola Superior d'Enginyeries Industrial,
Aeroespacial i Audiovisual de Terrassa

Interplanetary trajectories Patched Conic Approximation (PCA)

Report

Degree: Master's degree in Aerospace Engineering

Course: 220301 - Aerodynamics, Flight and Orbital Mechanics

Delivery date: 15-01-2018

Students: Fontanes Molina, Pol; Martínez Viol, Víctor; Urbano González, Eva María

Contents

List of Tables	iii
List of Figures	v
1 Aim	1
2 Theoretical background	2
2.1 Planetary orbits and approximations analysis	2
2.1.1 Patched Conic Approximation (PCA)	2
2.1.1.1 1st. Geocentric stage	3
2.1.1.2 2nd. Heliocentric stage	6
2.1.1.3 3rd. Planetocentric stage	12
3 Calculations and results	13
3.1 Verification	13
3.1.1 From Earth to Mars using an elliptic heliocentric trajectory	13
3.1.2 From Mars to Jupiter using an elliptic heliocentric trajectory	14
3.1.3 From Earth to Mars using an hyperbolic heliocentric trajectory	15
3.1.4 Verification conclusions	16
3.2 Main interplanetary orbit calculations	16
3.2.1 Case 1: Mars to Jupiter	17
3.2.2 Case 2: Earth to Mars	17
3.2.3 Case 3: Earth to Mars	18
3.2.4 Case 4: Earth to Mars	18
3.2.5 Case 5: Earth to Venus	19
3.2.6 Case 6: Mars to Earth	19
3.2.7 Case 7: Mars to Earth	20
3.2.8 Case 8: Earth to Mars (hyperbolic)	20
3.2.9 Case 9: Earth to Mars (hyperbolic)	21
3.3 Complementary calculations	21
3.3.1 Earth SOI scape parameters	21
3.3.2 Launch windows computation	22
4 Conclusions	23

CONTENTS

5 Bibliography	24
A Developed algorithms	25
A.1 Main code purpose and algorithm	25
A.2 Secondary parameters code	25
A.2.1 Hyperbolic scape geocentric velocities	26
A.2.2 Launch windows	26

List of Tables

2.1.1	Radius of influence of the planets	3
3.1.1	Data provided by the first example	13
3.1.2	Results provided by the first example	13
3.1.3	Results computed by the code developed for the first example	14
3.1.4	Relative error in the first example	14
3.1.5	Data provided by the second example	14
3.1.6	Results provided by the second example	14
3.1.7	Results computed by the code developed for the second example	15
3.1.8	Relative error in the second example	15
3.1.9	Data provided by the third example	15
3.1.10	Results provided by the third example	15
3.1.11	Results computed by the code developed for the third example	16
3.1.12	Relative error in the third example	16
3.2.1	Data provided for a travel between Mars and Jupiter	17
3.2.2	Results computed for a travel between Mars and Jupiter	17
3.2.3	Data provided for case 2	17
3.2.4	Results computed for case 2	17
3.2.5	Data provided for case 3	18
3.2.6	Results computed for case 3	18
3.2.7	Data provided for case 4	18
3.2.8	Results computed for case 4	18
3.2.9	Data provided for case 5	19
3.2.10	Results computed for case 5	19
3.2.11	Data provided for case 6	19
3.2.12	Results computed for case 6	19
3.2.13	Data provided for case 7	20
3.2.14	Results computed for case 7	20
3.2.15	Data provided for case 8	20
3.2.16	Results computed for case 8	20
3.2.17	Data provided for case 9	21
3.2.18	Results computed for case 9	21
3.3.1	Data provided for first example plus assumptions	21

LIST OF TABLES

3.3.2 Calculated parameter for the planetary scape. 22

List of Figures

2.1.1 Hyperbola Parameters. Extracted from [3]. 4

2.1.2 Velocities frames of reference. Extracted from [1] 5

2.1.3 Injection points circle. Extracted from [1] 6

2.1.4 Flow chart for the elliptic trajectory resolution. 9

2.1.5 Flow chart for the hyperbolic trajectory resolution. 10

2.1.6 ECI-*IJK* system, extracted from [1]. 11

1 | Aim

This project aims to compute an interplanetary trajectory which, for a given ecliptic rectangular positions of two planets in two known time instances, is able to carry a spaceship with a unique impulse, from the first planet to the second.

2 | Theoretical background

2.1 Planetary orbits and approximations analysis

In order to calculate the interplanetary trajectory between two planets, several approximations can be used. The simplest approximation, which can be called *aprox. 0* accepts the following hypothesis:

- Circular and coplanar orbits
- No analysis about the exit of the planet of start is done.
- No analysis about entering the planet of arrival is done.

Aprox. 0 is very basic and can be easily improved adding some parameters.

Another approximation widely used is **Patched Conic Approximation (PCA)**. This method improves significantly the results obtained with *aprox. 0* and represents a good starting point for a more precise numerical analysis of the mission. For this reason, in this project the PCA method will be used.

2.1.1 Patched Conic Approximation (PCA)

The Patched Conic Approximation (PCA) consist on the evaluation of an interplanetary trajectory dividing it into three stages. Considering the Earth as the planet of start, this stages are:

- Geocentric phase: Hyperbolic exit of the Earth. This phase takes place while the probe is going through the influence sphere of the Earth.
- Heliocentric phase: Trajectory with the Sun as main influencer.

Planetary orbits and approximations analysis

- Planet-centred phase: Hyperbolic arrival to the planet of destination. Similarly to the geocentric phase, this phase starts when the probe enters the sphere of influence of the planet.

The influence spheres mentioned are the space close to the planets where it can be considered that the influence of the Sun is negligible in comparison with that of the planet in question. The Laplace criteria will be considered to calculate this sphere. In Table 2.1.1 the radius of the sphere of influence of the solar system's planets are shown.

Planet	$R_I \times 10^6 \text{ km}$	$R_I \times 10^{-3} \text{ UA}$	R_I Radius of the planet
Mercury	0.111	0.740	45
Venus	0.616	4.11	100
Earth	0.924	6.16	145
Mars	0.577	3.85	170
Jupiter	48.157	321.0	677
Saturn	54.796	365.3	901
Uranus	91.954	346.4	2025
Neptune	80.196	534.6	3866

Table 2.1.1: Radius of influence of the planets

In order to set out the problem and begin with the resolution of it using the PCA method, the times and positions of the planets at the beginning and end of the trajectory are needed and some hypothesis are taken under consideration. The hypothesis are:

- The spheres of influences of the planets are not considered during the heliocentric phase. This hypothesis is admissible because the radius of the sphere are very small in comparison with the distance between planets.
- The spheres of influence are considered infinite from the point of view of the planet. This is assumed due to the fact that the radius of influence of the planets are much larger than the radius of the planet itself, as can be seen in Tabl 2.1.1.
- The duration of the trajectory can be taken as the duration of the heliocentric phase.

With this data the trajectory can be found through the orbital elements of the trajectories and the thrust required.

2.1.1.1 1st. Geocentric stage

This first stage of the trajectory of the probe aims to escape the gravitational field exerted by the departure planet. To achieve this, it is necessary to follow a hyperbolic trajectory that

guarantees to pass through the planet sphere of influence with a relative velocity V_∞ (also known as hyperbolic excess velocity).

Therefore, in this section necessary equations to characterize this hyperbola will be reviewed. Figure 2.1.1 shows the aforementioned situation. From the figure, it can be inferred that the hyperbola is defined by:

- C : Center of the hyperbola.
- β : Angle of the hyperbola.
- b : Exit parameter.

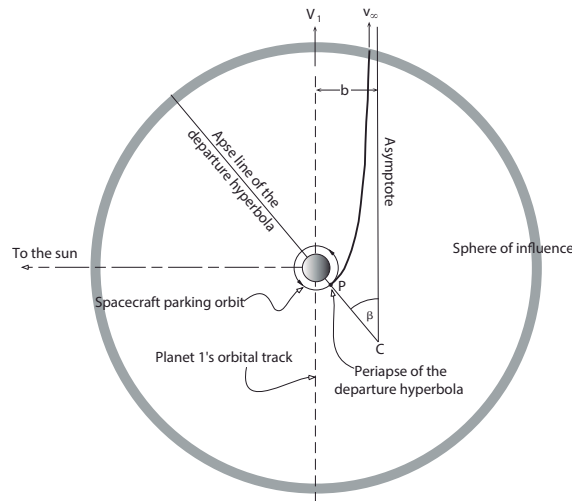


Figure 2.1.1: Hyperbola Parameters. Extracted from [3].

The hyperbola can also be defined by the semi-major axis (a) and the eccentricity (e). In addition, the ΔV necessary to inject the probe into the hyperbolic orbit from the parking orbit must be specified.

To obtain these parameters, only the heliocentric departure speed (v_1), the velocity of the departure planet (v_p) and the parking orbit (in particular, the periapse radius and the speed of the orbit) are needed.

Definition of hyperbola: The first step is to obtain the semi-major axis of the hyperbola. This is obtained from the hyperbolic excess velocity as:

$$a = \frac{\mu}{V_\infty^2} \quad (2.1.1)$$

where μ is the standard gravitational parameter ($\mu = GM$) for the sun and the excess velocity is computed as the difference between the probe velocity and the departure planet speed. The eccentricity of hyperbola is defined by:

$$e = 1 + \left(\frac{V_\infty}{V_0} \right)^2 \quad (2.1.2)$$

where V_0 refers to the speed of the parking orbit. If this orbit is assumed to be circular with r_0 as the periapse, the probe velocity through the parking orbit is given by:

$$V_0 = \sqrt{\frac{\mu_0}{r_0}} \quad (2.1.3)$$

being μ_0 the standard gravitational parameter of the departure planet. Once the eccentricity is computed, the beta angle is easily obtained as:

$$\cos \beta = \frac{1}{e} \quad (2.1.4)$$

Finally, the exit parameter is computed by means of:

$$b = a\sqrt{e^2 - 1} \quad (2.1.5)$$

Obtaining the center of the hyperbola is a little bit more cumbersome. Given the three velocities (V_∞ , v_p and v_1), the two frames of the figure 2.1.2 can be defined. One has the Y-axis in the direction of the planet velocity and the other has the vernal point over the X-axis. Then, the angle between the planet velocity and this X-axis is defined as $\lambda_v = 90 + \lambda_x$. Determining this λ_x at the injection time t_1 allows us to obtain the right ascension (α) and the declination (δ) of the v_1 velocity by means of a change of frame:

$$\begin{bmatrix} V_\infty \end{bmatrix}_Q = \mathcal{R}_1(-\varepsilon) \mathcal{R}_3(-\lambda_x) \begin{bmatrix} V_\infty \end{bmatrix}_K \quad (2.1.6)$$

Thus,

$$\sin \delta = [V_z]_Q; \quad \tan \alpha = \left[\frac{V_y}{V_x} \right]_Q \quad (2.1.7)$$

Finally, the center of the hyperbola has the following coordinates $(\alpha + 12^h, \delta)$.

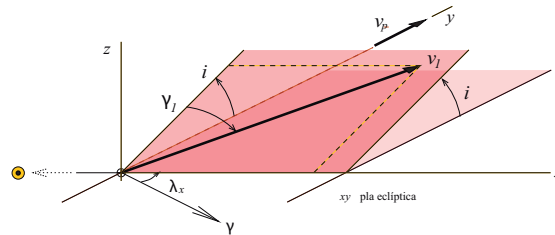


Figure 2.1.2: Velocities frames of reference. Extracted from [1]

Delta-v determination The necessary delta-v to put the probe onto the hyperbolic departure trajectory is given by:

$$\Delta V = v_p - V_0 = \sqrt{V_\infty + 2V_0} - V_0 \quad (2.1.8)$$

The only requirement of the plane of the departure hyperbola is that it must contain the planet center of mass as well as the hyperbolic excess velocity. Therefore, the delta-v has to be applied once the probe flies over C, at a distance of $r_0 \sin \beta$. The circle of all the possible perigees is the injection points circle.

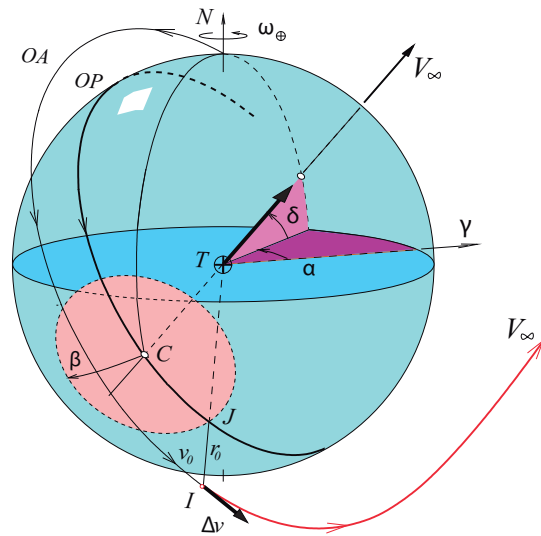


Figure 2.1.3: Injection points circle. Extracted from [1]

2.1.1.2 2nd. Heliocentric stage

In this section the equations and assumptions done in order to obtain the orbital elements of the trajectory will be explained. The objective of the calculations done regarding this stage is to find:

- Ω : Right ascension of the ascending node.
- e : Eccentricity.
- i : Inclination to the ecliptic plane.
- a : Semimajor axis.
- ω : Argument of the perihelion.

As said previously, the times of departure and arrival are provided, together with the position of the planets. The steps to be followed to achieve the aim of this section are now explained.

Longitude, latitude and distance The position vector is defined as:

$$\vec{r} = (x_k, y_k, z_k) \quad (2.1.9)$$

Where:

$$x_k = r \cos \beta \cos \lambda \quad (2.1.10)$$

$$y_k = r \cos \beta \sin \lambda \quad (2.1.11)$$

$$z_k = r \sin \beta \quad (2.1.12)$$

Then longitude, latitude and distance are computed with:

$$r = |\vec{r}| \quad (2.1.13)$$

$$\beta = \arcsin\left(\frac{z_k}{r}\right) \quad (2.1.14)$$

$$\lambda = \arctan\left(\frac{y_k}{x_k}\right) \quad (2.1.15)$$

The difference between λ at the beginning and at the end of the trajectory is an important magnitude that will be used. Taking into account that subscript 1 refers to the start position and subscript 2 to the end:

$$\Delta\lambda = \lambda_2 - \lambda_1 \quad (2.1.16)$$

Inclination, right ascension of the ascending node and true anomaly variation

Trigonometry has to be used to compute this elements. A general case will be considered, that is to say, that no assumption will be done on whether the two planets are on the ecliptic or not. As shown in reference [1], the equations to be used are:

$$\cos \Delta\theta = \sin \beta_1 \sin \beta_2 + \cos \beta_1 \cos \beta_2 \cos \Delta\lambda \quad (2.1.17)$$

$$\sin A = \cos \beta_2 \frac{\sin \Delta\lambda}{\sin \Delta\theta} \quad (2.1.18)$$

$$\cos i = \sin A \cos \beta_1 \quad (2.1.19)$$

$$\sin l = \frac{\tan \beta_1}{\tan i} \quad (2.1.20)$$

$$\tan \sigma = \frac{\tan \beta_1}{\cos A} \quad (2.1.21)$$

$$\Omega = \lambda_1 - l \quad (2.1.22)$$

Eccentricity, semimajor axis and true anomaly of the starting point With the aim of obtaining this data three equations can be stated. Due to the complexity of the equations, the resolution will be done iteratively. Two cases will be considered: elliptic and hyperbolic. Its equations and iteration process are now shown:

- Elliptic trajectory: The equations of the elliptic trajectory are:

$$e = \frac{r_2 - r_1}{r_1 \cos \theta_1 - r_2 \cos(\theta_1 + \Delta\theta)} \quad (2.1.23)$$

$$a = \frac{r_1 (1 + e \cos \theta_1)}{1 - e^2} \quad (2.1.24)$$

$$t_2 - t_1 = \frac{365.25}{2\pi} a^{\frac{3}{2}} \left(2 \arctan \left(\sqrt{\frac{1-e}{1+e}} \tan \frac{\theta_1 + \Delta\theta}{2} \right) - \frac{e \sqrt{1-e^2} \sin(\theta_1 + \Delta\theta)}{1 + e \cos(\theta_1 + \Delta\theta)} - 2 \arctan \left(\sqrt{\frac{1-e}{1+e}} \tan \frac{\theta_1}{2} \right) + \frac{e \sqrt{1-e^2} \sin \theta_1}{1 + e \cos \theta_1} \right) \quad (2.1.25)$$

The iteration process done to solve the equations will deal with the difference between the time of the mission calculated and the real time of the mission, that is a known value. An error criteria ϵ is defined as the convergence value. Since the convergence criteria gives a difference in terms of time and the tuning parameter is an angle, there is no possibility to develop an adaptive increase step for θ_1 (due to their completely different physical meaning). However, a kind of *intelligent* convergence can be applied involving the sign of the time difference multiplying the θ step by the time error and dividing it by the time error absolute value.

Another issue related to the algorithm based on tuning an angle is the possibility of entering into a loop between two results if the step used is not small enough. To solve this problem, the algorithm includes a procedure to detect this situation and reduce the θ step in order to avoid the loop. The flow chart of this iteration (without the details of the aforementioned convergence system) is shown in Figure 2.1.4.

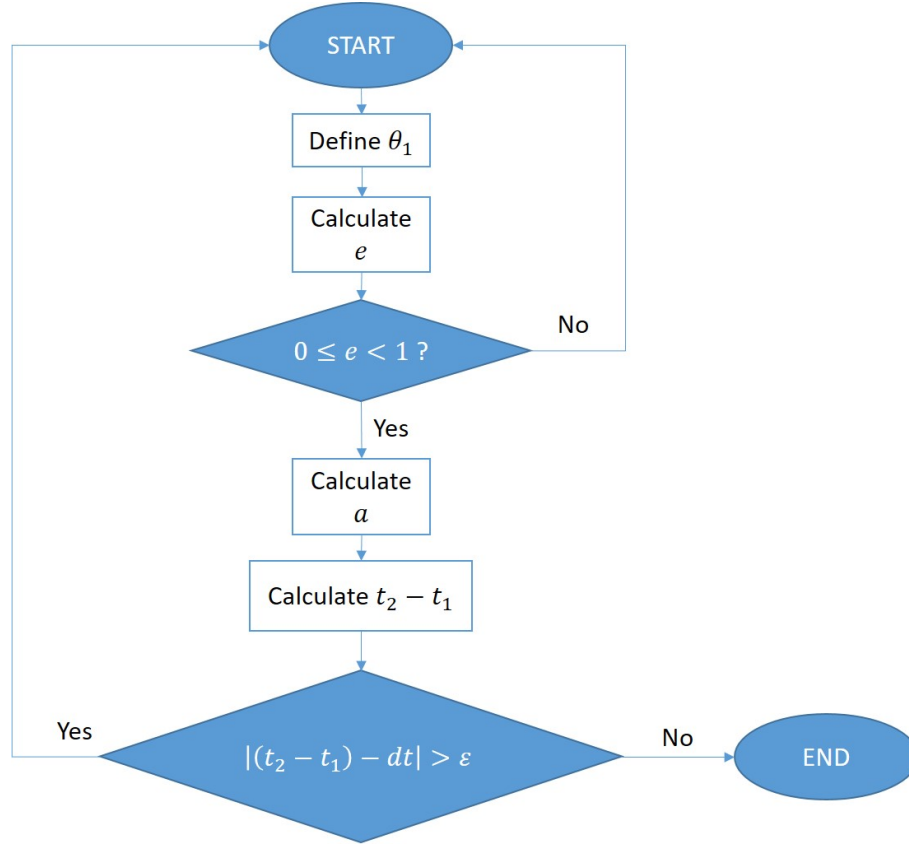


Figure 2.1.4: Flow chart for the elliptic trajectory resolution.

- Hyperbolic trajectory: The equations of the hyperbolic trajectory are:

$$e = \frac{r_2 - r_1}{r_1 \cos \theta_1 - r_2 \cos(\theta_1 + \Delta\theta)} \quad (2.1.26)$$

$$a = \frac{r_1 (1 + e \cos \theta_1)}{e^2 - 1} \quad (2.1.27)$$

$$t_2 - t_1 = \frac{365.25}{2\pi} a^{\frac{3}{2}} \left(\frac{e\sqrt{e^2 - 1} \sin(\theta_1 + \Delta\theta)}{1 + e \cos(\theta_1 + \Delta\theta)} - \ln \left| \frac{\tan \frac{\theta_1 + \Delta\theta}{2} + \sqrt{\frac{e+1}{e-1}}}{\tan \frac{\theta_1 + \Delta\theta}{2} - \sqrt{\frac{e+1}{e-1}}} \right| - \frac{e\sqrt{e^2 - 1} \sin \theta_1}{1 + e \cos \theta_1} + \ln \left| \frac{\tan \frac{\theta_1}{2} + \sqrt{\frac{e+1}{e-1}}}{\tan \frac{\theta_1}{2} - \sqrt{\frac{e+1}{e-1}}} \right| \right) \quad (2.1.28)$$

The resolution is similar to that of the elliptic case, but the acceptable values of the eccentricity change. The flow chart is shown in Figure 2.1.5.

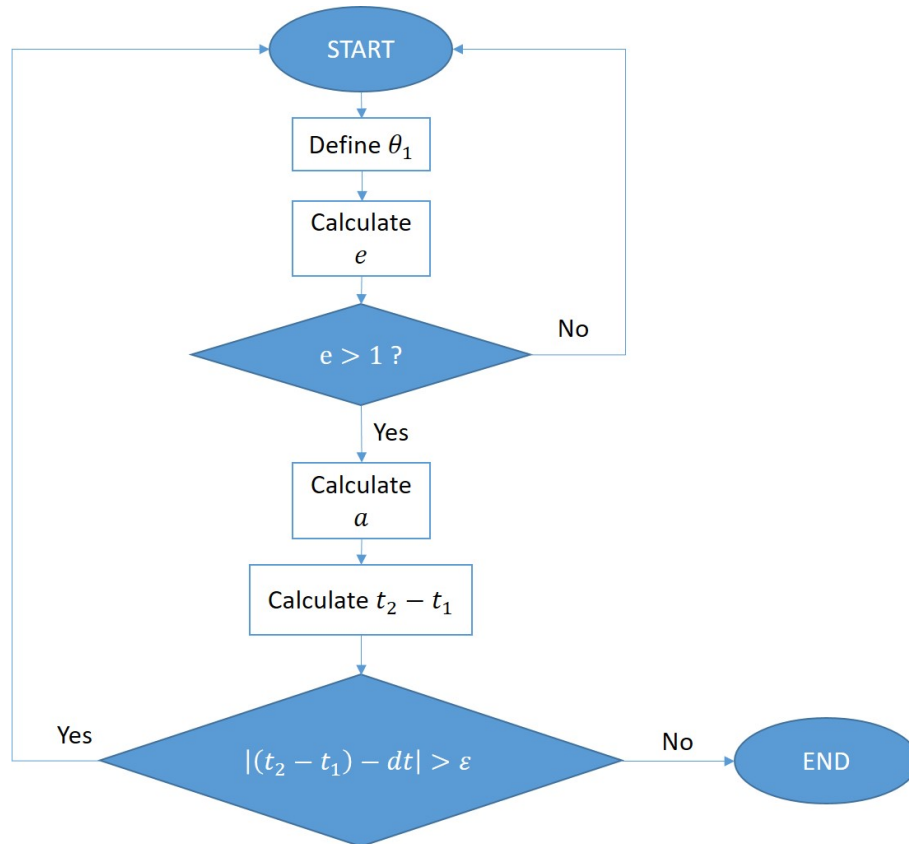


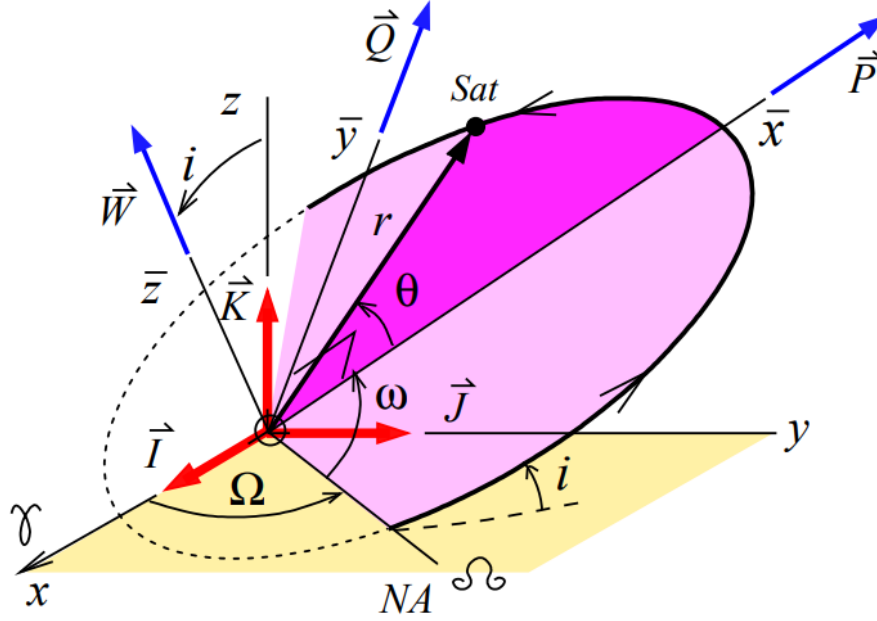
Figure 2.1.5: Flow chart for the hyperbolic trajectory resolution.

Argument of the perihelion The only remaining orbit element that needs to be computed is ω . It can be calculated using results from the previous steps:

$$\omega = 2\pi - (\theta_1 - \sigma) \quad (2.1.29)$$

Spacecraft velocity Sphere Of Influence (SOI), departure and arrival velocities are computed under the following theoretical background.

First of all, a geocentric coordinates system is considered with the orbital plane $PQW(\bar{x}, \bar{y}, \bar{z})$. The spacecraft orbit is situated on the system $ECI-IJK$, seen on the following figure.


 Figure 2.1.6: ECI-*IJK* system, extracted from [1].

A series of rotations are done, for changing from the orbital plane *PQW* to the equatorial *IJK*. A, \mathbb{M} rotation matrix is defined:

$$\mathbb{M}(\omega, i, \Omega) = \mathbb{R}_3(-\Omega) \cdot \mathbb{R}_3(-i) \cdot \mathbb{R}_3(-\omega)$$

with the following components:

$$\begin{aligned} \mathbb{M}_{11} &= P_x = +\cos \Omega \cos \omega - \sin \Omega \cos i \sin \omega \\ \mathbb{M}_{21} &= P_y = +\sin \Omega \cos \omega + \cos \Omega \cos i \sin \omega \\ \mathbb{M}_{31} &= P_z = \sin i \sin \omega \\ \mathbb{M}_{12} &= Q_x = -\cos \Omega \sin \omega - \sin \Omega \cos i \cos \omega \\ \mathbb{M}_{22} &= Q_y = -\sin \Omega \sin \omega + \cos \Omega \cos i \cos \omega \\ \mathbb{M}_{32} &= Q_z = +\sin i \cos \omega \\ \mathbb{M}_{13} &= W_x = +\sin \Omega \sin i \\ \mathbb{M}_{23} &= W_y = -\cos \Omega \sin i \\ \mathbb{M}_{33} &= W_z = +\cos i \end{aligned} \tag{2.1.30}$$

Therefore, spacecraft geocentric position vector \vec{r} is:

$$\vec{r} = \bar{x}\vec{P} + \bar{y}\vec{Q} = x\vec{I} + y\vec{J} + z\vec{K} \tag{2.1.31}$$

with

$$\vec{P} = P_X\vec{I} + P_Y\vec{J} + P_Z\vec{K} \tag{2.1.32}$$

Finally, heliocentric \vec{r} and $\dot{\vec{r}}$ can be computed using \vec{P} , \vec{Q} , \vec{W} unitary vectors, as

$$\vec{r} = r[\cos \theta \cdot \vec{P} + \sin \theta \cdot \vec{Q}] \quad (2.1.33)$$

$$\dot{\vec{r}} = \sqrt{\frac{\mu_{\odot}}{p}}[-\sin \theta \cdot \vec{P} + (e + \cos \theta) \cdot \vec{Q}] \quad (2.1.34)$$

taking into account that parameter p is $p = a(1 - e^2)$ for elliptic trajectories and $p = a(e^2 - 1)$ for hyperbolic ones.

Also for computing \vec{r} and $\dot{\vec{r}}$ for the departure and arrival cases, θ , the true anomaly is

$$\text{Departing SOI: } \theta = \theta_0 \quad \text{Arriving SOI: } \theta = \theta_1 = \theta_0 + \Delta\theta$$

In conclusion, for calculating the spacecraft heliocentric departure and arrival velocities to the SOI of each planet, previously the heliocentric orbital elements would have to be calculated following the equations exposed before the velocity paragraph. Because, for this study the planets position vectors are given, we can verify the correction of velocity equations $\dot{\vec{r}}$, comparing the given position vector with the one calculated, \vec{r} , they should match.

2.1.1.3 3rd. Planetocentric stage

Once the spacecraft, enter into the SOI of the destination planet, the planetocentric stage starts. The spacecraft, describes a planet arrival hyperbola. Depending of the arrival velocity and position three main scenarios can be described for the spacecraft.

Impact If arrival position $r_p \leq R_P$.

Slowdown Atmosphere interaction will slowdown the spacecraft if $r_p \leq R_a$.

Flyby Spacecraft will perform a flyby over the planet if $r_p > R_a$ or $b > b_a$.

Note that R_P and R_a , correspond to the planet and atmosphere radius respectively.

The spacecraft, will only stay trapped on the destination planet, orbiting, if the spaceship has slowdown enough in contact with the planet atmosphere or the spaceship braked during the periastron.

Because, the main assignment objective was to calculate, a trajectory between to planets for interplanetary travel. This stage is been only develop theoretically, expressions for computing theses parameters can be obtained on, [1]. First and third stage of the PCA, share some concepts and equations because in both, an hyperbolic trajectory is performed.

3 | Calculations and results

3.1 Verification

In order to verify the code, examples shown at reference [2] will be used. In this section, the results provided for every example will be exposed together with the results obtained using the code developed for this project and conclusions will be extracted.

3.1.1 From Earth to Mars using an elliptic heliocentric trajectory

Departure date	2020 Jul 19
Arrival date	2021 Gen 25
Δt	190 days
r_1	(0.4537, -0.9094, 0.0000)AU
r_2	(0.3148, 1.5078, 0.0239)AU

Table 3.1.1: Data provided by the first example

Semimajor axis	1.33069 AU
Eccentricity	0.23629
θ_0	359.621°
ω	0.470°
Inclination	1.435°
Ω	296.424°
Heliocentric velocity at departure (km/s)	(29.3678, 14.6982, 0.8229)
Heliocentric velocity at arrival (km/s)	(20.4069, 8.2271, 0.3656)

Table 3.1.2: Results provided by the first example

Semimajor axis	1.33073 AU
Eccentricity	0.236291
θ_0	359.613°
ω	0.386861°
Inclination	1.43388°
Ω	296.515°
Heliocentric velocity at departure (km/s)	(29.367, 14.6986, 0.822024)
Heliocentric velocity at arrival (km/s)	(-20.4068, 8.27743, -0.364583)

Table 3.1.3: Results computed by the code developed for the first example

Parameter	Relative error (%)
a	0.0030
e	0.0004
θ_0	0.0022
ω	17.6891
i	0.0780
Ω	0.0307
v_{t_1}	0.0017
v_{t_1}	0.0001

Table 3.1.4: Relative error in the first example

3.1.2 From Mars to Jupiter using an elliptic heliocentric trajectory

Departure date	2026 Jun 05
Arrival date	2029 April 25
Δt	1055 days
r_1	(1.3277, 0.4901, 0.0223)AU
r_2	(5.0135, 2.1380, 0.0505)AU

Table 3.1.5: Data provided by the second example

Semimajor axis	3.45403 AU
Eccentricity	0.59218
θ_0	350.769°
ω	182.312°
Inclination	7.513°
Ω	207.121°
Heliocentric velocity at departure (km/s)	(12.5324, 28.6817, 4.1200)
Heliocentric velocity at arrival (km/s)	(1.9715, 7.9799, 1.0552)

Table 3.1.6: Results provided by the second example

Semimajor axis	3.45405
Eccentricity	0.592181
θ_0	350.469°
ω	196.156°
Inclination	7.508444°
Ω	207.127°
Heliocentric velocity at departure (km/s)	(-19.0894, 24.8148, -4.05809)
Heliocentric velocity at arrival (km/s)	(3.83725, -7.26513, 1.08284)

Table 3.1.7: Results computed by the code developed for the second example

Parameter	Relative error (%)
a	0.0006
e	0.0002
θ_0	0.0000
ω	7.5936
i	0.0606
Ω	0.0029
v_{t_1}	0.0014
v_{t_1}	0.0001

Table 3.1.8: Relative error in the second example

3.1.3 From Earth to Mars using an hyperbolic heliocentric trajectory

Departure date	2020 Mar 06
Arrival date	2020 Jun 09
Δt	95 days
r_1	(-0.9609, 0.2466, 0.0000)AU
r_2	(0.7285, -1.1980, -0.0430)AU

Table 3.1.9: Data provided by the third example

Semimajor axis	71.08581 AU
Eccentricity	1.01113
θ_0	-53.310°
ω	233.297°
Inclination	2.513°
Ω	345.619°
Heliocentric velocity at departure (km/s)	(9.1364, -41.4090, -1.6612)
Heliocentric velocity at arrival (km/s)	(35.1754, -6.3201, 0.1148)

Table 3.1.10: Results provided by the third example

Main interplanetary orbit calculations

Semimajor axis	71.6165
Eccentricity	1.01105
θ_0	306.691°
ω	233.309°
Inclination	2.51416°
Ω	345.607°
Heliocentric velocity at departure (km/s)	(9.13562,-41.4082,-1.66139)
Heliocentric velocity at arrival (km/s)	(35.1747,-6.31841,0.115199)

Table 3.1.11: Results computed by the code developed for the third example

Parameter	Relative error (%)
a	0.7465
e	0.0079
θ_0	0.0003
ω	0.0051
i	0.0462
Ω	0.0035
v_{t_1}	0.1189
v_{t_1}	0.0028

Table 3.1.12: Relative error in the third example

3.1.4 Verification conclusions

It can be appreciated that in most of the cases the relative error is far less than one. The highest error produced is less than 17%, and its cause probably deal with the equations and assumptions done while computing the results.

Although, heliocentric arrival and departure velocities, may differ in some sign for one of the components. After an extensive study, is determined that could be, because of the angles definition. This opposite values, show that the vector obtained is just the symmetric, that is equivalent to the solution if angles are chosen accordingly

Therefore, the code is taken as valid and can be used in order to obtain other interplanetary trajectories. It has been designed in a general manner so the same code can compute elliptic and hyperbolic trajectories with any departure and arrival planet in the solar system.

3.2 Main interplanetary orbit calculations

Following, the cases proposed in reference [2] will be solved.

3.2.1 Case 1: Mars to Jupiter

Departure date	2037 Oct 25
Arrival date	2039 Oct 15
Δt	720 days
r_1	(1.0707, 0.9868, 0.0055)
r_2	(5.2210, 1.4357, 0.1109)

Table 3.2.1: Data provided for a travel between Mars and Jupiter

Semimajor axis	4.27012 AU
Eccentricity	0.725509
θ_0	302.422 °
ω	63.3568°
Inclination	2.14985°
Ω	36.89°
Heliocentric velocity at departure (km/s)	(-29.1352, 12.6808, 1.03727)
Heliocentric velocity at arrival (km/s)	(4.72014, -9.86931, -0.402679)

Table 3.2.2: Results computed for a travel between Mars and Jupiter

3.2.2 Case 2: Earth to Mars

Departure date	2033 Mar 13
Arrival date	2033 Aug 05
Δt	145 days
r_1	(0.9848, 0.1338, 0.0000)
r_2	(0.6797, 1.2298, 0.0424)

Table 3.2.3: Data provided for case 2

Semimajor axis	1.37053 AU
Eccentricity	0.615632
θ_0	256.507°
ω	103.493°
Inclination	2.15438°
Ω	7.73712°
Heliocentric velocity at departure (km/s)	(-22.8707, 24.7746, 1.03934)
Heliocentric velocity at arrival (km/s)	(9.73264, -22.7879, -0.898741)

Table 3.2.4: Results computed for case 2

3.2.3 Case 3: Earth to Mars

Departure date	2031 Jan 23
Arrival date	2031 Aug 01
Δt	190 days
r_1	(0.5264, 0.8316, 0.0001)
r_2	(0.0108, 1.4542, 0.0309)

Table 3.2.5: Data provided for case 3

Semimajor axis	1.24706 AU
Eccentricity	0.381113
θ_0	282.584 °
ω	77.5612 °
Inclination	2.29274 °
Ω	57.8117 °
Heliocentric velocity at departure (km/s)	(-48.5598, 30.3938, 2.29362)
Heliocentric velocity at arrival (km/s)	(20.646, -0.03366, -0.70028)

Table 3.2.6: Results computed for case 3

3.2.4 Case 4: Earth to Mars

Departure date	2025 Jul 18
Arrival date	2025 Oct 21
Δt	95 days
r_1	(0.4342, 0.9188, 0.0001)
r_2	(0.6775, 1.3571, 0.0118)

Table 3.2.7: Data provided for case 4

Semimajor axis	122.519 AU
Eccentricity	-1.0008
θ_0	360.052°
ω	-0.0356°
Inclination	19.6087°
Ω	64.7217°
Heliocentric velocity at departure (km/s)	-
Heliocentric velocity at arrival (km/s)	-

Table 3.2.8: Results computed for case 4

Results partially converged. Code, doesn't perform well in this case.

3.2.5 Case 5: Earth to Venus

Departure date	2023 May 27
Arrival date	2023 Nov 01
Δt	158 days
r_1	(-0.4255, -0.9194, 0.0000)
r_2	(0.0356, 0.7189, 0.0079)

Table 3.2.9: Data provided for case 5

Semimajor axis	217.426 AU
Eccentricity	-0.847689
θ_0	360.007 °
ω	-0.00657141 °
Inclination	1.67824 °
Ω	245.165 °
Heliocentric velocity at departure (km/s)	(2.45241, -1.13498, 0.0791754)
Heliocentric velocity at arrival (km/s)	(4.80202, -5.12288, 0.190725)

Table 3.2.10: Results computed for case 5

3.2.6 Case 6: Mars to Earth

Departure date	2033 Jan 18
Arrival date	2033 Aug 28
Δt	222 days
r_1	(1.5831, 0.3913, 0.0306)
r_2	(0.9123, 0.4340, 0.0000)

Table 3.2.11: Data provided for case 6

Semimajor axis	1.31867 AU
Eccentricity	0.236873
θ_0	180 °
ω	371.607 °
Inclination	5.3505 °
Ω	205.441 °
Heliocentric velocity at departure (km/s)	(-6.43846, 8.513846, -0.97904)
Heliocentric velocity at arrival (km/s)	(32.4436, -28.4563, 3.71199)

Table 3.2.12: Results computed for case 6

3.2.7 Case 7: Mars to Earth

Departure date	2030 Nov 20
Arrival date	2031 Jul 06
Δt	228 days
r_1	(1.4166, 0.8722, 0.0530)
r_2	(0.2345, 0.9893, 0.0001)

Table 3.2.13: Data provided for case 7

Semimajor axis	1.30864 AU
Eccentricity	0.271869
θ_0	180 °
ω	405.199 °
Inclination	2.57215 °
Ω	256.79 °
Heliocentric velocity at departure (km/s)	(-9.20594, -5.75652, -0.343519)
Heliocentric velocity at arrival (km/s)	(0.111769, 0.4865, -0.000106258)

Table 3.2.14: Results computed for case 7

3.2.8 Case 8: Earth to Mars (hyperbolic)

Departure date	2021 Nov 26
Arrival date	2022 Feb 19
Δt	85 days
r_1	(0.4383, 0.8843, 0.0000)
r_2	(-0.2082, -1.4582, -0.0255)

Table 3.2.15: Data provided for case 8

Semimajor axis	1.34023 AU
Eccentricity	1.44255
θ_0	288.925 °
ω	251.075 °
Inclination	3.16587 °
Ω	243.635 °
Heliocentric velocity at departure (km/s)	(0.322509, 0.650683, 0)
Heliocentric velocity at arrival (km/s)	(-1.20802, -1.22481, -0.0297817)

Table 3.2.16: Results computed for case 8

Complementary calculations

3.2.9 Case 9: Earth to Mars (hyperbolic)

Departure date	2022 Jan 15
Arrival date	2022 Apr 20
Δt	95 days
r_1	(-0.4079, 0.8950, 0.0000)
r_2	(0.6393, -1.2542, -0.0420)

Table 3.2.17: Data provided for case 9

Semimajor axis	5.10169 AU
Eccentricity	1.11068
θ_0	280.991 °
ω	259.009 °
Inclination	34.288 °
Ω	294.501 °
Heliocentric velocity at departure (km/s)	(-16.804 , -7.65848 , -12.5916)
Heliocentric velocity at arrival (km/s)	(36.9836 , 14.0711 , 26.9253)

Table 3.2.18: Results computed for case 9

3.3 Complementary calculations

3.3.1 Earth SOI scape parameters

Applying the equations from the 1st geocentric stage, of the PCA. The first given example, Earth to Mars trip, planetary departure parameters are determined.

Departure date	2020 Jul 19
Arrival date	2021 Gen 25
Δt	190 days
r_0	300 km
I_{sp}	300 s

Table 3.3.1: Data provided for first example plus assumptions

Note that r_0 is the initial circular parking orbit of the spacecraft and I_{sp} is the specific impulse.

Complementary calculations

Hyperbolic excess speed, v_∞	2.9439 km/s
Spacecraft speed on parking orbit, v_c	7.7298 km/s
Δv	3.5912 km/s
Perigee of departure hyperbola	6671 km
β	29.1525 °
Spacecraft fuel percent among total mass	70.48 %

Table 3.3.2: Calculated parameter for the planetary scape.

Spacecraft fuel percent among total mass is calculated as

$$\%m_{fuel} = 1 - e^{\left(-\frac{\Delta v}{I_{sp}g_0}\right)} \quad (3.3.1)$$

and for this particular example means that the 70.48% of the total spacecraft weight will be the fuel that will burn in order to scape the Earth SOI.

3.3.2 Launch windows computation

For the first given example, Earth to Mars trip, same used in the previous section, the launch window is computed using the algorithm from the appendix A.2.2.

$$C = (15.9199^h, 0.6188rad) \quad R = 3.2497 \cdot 10^3 km$$

C is given in equatorial coordinates.

These results indicates the area (from radius R) where the spacecraft can leave Earth and where it needs to apply the impulse (C point). Knowing the launching site, the launch window availability time could be computed.

This calculus is generic and could be computed for all studied cases. All parameters are extracted from the main code and planetary departure code, but the Earth heliocentric velocity is computed with [3] equations and checked with the given by NASA ephemerides.

4 | Conclusions

After performing this project, it can be said that orbital mechanics is not a trivial matter. This project, have been hard to start, because it took us some time to be familiar with the concepts and how they are explained through the equations. Finally, after this project, we understand the patched conics approximation development and hypothesis.

It has not been easy to implement the method explained during the lessons, mostly because at some point if concepts weren't clear enough, the convergence sections of the code, failed to give a solution. Getting the code working well to verify the examples, excited us, we feel confident to have consistent results. After this personal thoughts introduction we can extract some technical conclusions.

Main code implemented, demonstrated to work optimally for trajectories departing Earth to outer planets. Both trajectories, elliptical and hyperbolic, have been correctly compute as seen on the code verification. Nevertheless, as more cases were tried more specific problems for each case appeared. This fact, lead us to improve the code at every simulation.

Comparing some results from book [3] examples with our code, in most cases parameters match. The code, only presents troubles calculating inner planets trajectories, most likely, because, proper exceptions for this trajectories have not been implemented yet.

One final thought, after computing these trajectories, it is seen that years for travelling to Mars are coming. Around 2022, trips to Mars from Earth will took really few days, around 100 days. This ideas totally matches with the fact that NASA and SpaceX, are developing their deep space exploration rockets for stepping humans into the red planet.

Finally, patched conics approximation, demonstrated that despite its complexity, it is a low computational effort method. These results will be taken as starting parameters for precise numerical integrations on real missions.

5 | Bibliography

- [1] Jaume Calaf. Trajectòries interplanetàries: Patched Conic Approximation. 2017.
- [2] Jaume Calaf. Treballs de Mecànica Orbital. 2017.
- [3] A.G Fallis. Orbital Mechanics for Engineering Students. *Journal of Chemical Information and Modeling*, 53(9):1689–1699, 2013.

A | Developed algorithms

All developed algorithm, had been computed with Matlab scripts. All of them, are attached together with the report, on a zip file for delivery. Following, developed algorithms concept and structure will be outlined.

A.1 Main code purpose and algorithm

Main code implemented, *Main_HeliocentricOrbitalElements.m*, calculates the heliocentric stage related parameters of the PCA, in a generic way. The implemented algorithm is:

1. **Load input data:** Obtain departure and arrival dates, fly time in days, planets heliocentric positions for the departing day and μ_{\odot} .
2. **Select kind of trajectory:** Trajectory can be elliptic or hyperbolic.
3. **Initial calculations:** Calculate $||\vec{r}||, \beta, \lambda, \Delta\lambda, \Omega, i, \sigma$.
4. **Iterate until convergence:** Find values e, a, θ_1 , by iterating the functions *Computeelliptic.m* for elliptic cases or *Computehyperbolic.m* for hyperbolic cases.
5. **Compute ω**
6. **Compute SOI arrival and departure velocities:** Find *PQW* parameters, for making the calculation.

A.2 Secondary parameters code

These codes have been develop parallel to the main code. They are use full for interesting interplanetary missions parameters, but they are not the main objective to develop on this assignment. That is why, they are treated apart.

A.2.1 Hyperbolic scape geocentric velocities

Based on the equations described for the geocentric phase for the patched conics approximation. This code, *Main_GeneralManoeuvres.m*, computes the hyperbolic excess speed, the spacecraft speed on a parking orbit, Δv , the perigee of departure hyperbola the beta angle and the spacecraft fuel percent among total mass.

A.2.2 Launch windows

This functions, *Main_LaunchWindows.m*, is meant to be integrated on the main code, and for a given launching location and exceeds velocity v_∞ , can determine the time and azimuths where the launch window is available.